Digital Applications in Archaeology and Cultural Heritage 30 (2023) e00273

Contents lists available at ScienceDirect

Digital Applications in Archaeology and Cultural Heritage

journal homepage: www.elsevier.com/locate/daach

3D printed control for commercial off-the-shelf (COTS) close-range photogrammetric reconstruction

Heather M. Tamminen *, Martin J. Smith, Kate Welham, Andrew L.J. Ford

Faculty of Science and Technology, Bournemouth University, UK

ARTICLE INFO

Keywords:
Photogrammetry
Archaeology
Biological anthropology
Forensic anthropology
3D printing
3D modelling

ABSTRACT

The use of photogrammetry in archaeology and anthropology has become increasingly popular over the past decade. If the intended purpose of a three-dimensional (3D) model generated by commercial "off-the-shelf" (COTS) photographic equipment is geometric analysis or preservation by record, appropriate 3D control is recommended to improve orientation estimates and, in turn, the accuracy of the output 3D model. Further, independent measures of the quality of the photogrammetric model (in addition to the 3D model output itself) are recommended for robust validation. This paper evaluates the use of bespoke 3D printed designs (cradles) to add both control points to close-range 3D model and check points for validation. There were no statistically significant differences between the control and check points errors and intra-observer error was low and comparable to conventional manual measurement methods, thus providing an accessible method of adding 3D control to close-range photogrammetry.

1. Introduction

Photogrammetric techniques are widespread in their uses, and now commonly applied to a variety of subjects such as archaeology, cultural heritage, ecology, geomorphology, engineering, and defence (e.g. Westoby et al., 2012; Olson et al., 2013; McCarthy 2014; Sapirstein 2018). Without three-dimensional (3D) documentation of archaeological sites and artefacts, context and important data that has been recorded can be lost (Ducke et al., 2011; De Reu et al., 2013, 2014; Dellepiane et al., 2013; Ashton et al., 2014; McCarthy 2014; Papworth et al., 2016; Porter et al., 2016; Sapirstein 2016; Sapirstein and Murray 2017; Magnani et al., 2020). Over a larger extent, virtual 3D records of sites can also aid in the reconstruction or approximation of the site. Where such archaeological or cultural heritage sites require monitoring (for instance of any on-going deterioration) control points are often required for co-registration of the resulting models (Linder 2016; Bartzis 2017; Cârlan and Dovleac 2017). The widespread adoption of photogrammetry also allows for more 3D records in fields that have conventionally used two-dimensional (2D) methods, such as artefact and bone recording (Bryan and Chandler 2008; Remondino 2011; Olson et al., 2013; McCarthy 2014; Evgenikou and Georgopoulos 2015; Clini et al., 2016; Porter et al., 2016; Bleed et al., 2017; Lauria et al., 2022). This paper focuses on the archaeological application of a novel method to ensure that small 3D models created through close-range photogrammetry with commercial "off-the-shelf" (COTS) equipment, either hand-held or tripod mounted, can be scaled and orientated accurately as well as more readily validated.

2. Background

When creating 3D visualisations through photogrammetry, the output can only ever match the quality of the input. The inputs are overlapping, stereo images (resulting in parallax), with the outputs consisting of one or more of the following: dense point clouds, meshes, digital elevation models (DEM), or orthophotographs (Konecny 1985; Luhmann et al., 2013; Lillesand et al., 2015; Linder 2016; Oniga et al., 2018). The quality of inputs does not relate solely to the capture of in-focus images at close-range with a suitable depth-of-field, but also reliable estimates of interior and exterior orientation. Interior orientation refers to camera parameters such as dimensions of the sensor array, the focal length and lens distortions. Exterior orientation refers to the 3D position (x, y and z) and rotation (ψ, θ and φ), also known as the camera's *pose.* The relationship between all these parameters is established by triangulation (also known as aerial- or aero-triangulation when used for aerial survey). Initial estimates of interior and exterior orientation may not exist, or there may be *a priori* estimates. In either case they are

* Corresponding author. Talbot Campus, Fern Barrow, Poole, BH12 5BB, UK.
E-mail address: heather.m.tamminen@gmail.com (H.M. Tamminen).

https://doi.org/10.1016/j.daach.2023.e00273
Received 4 October 2022; Received in revised form 26 February 2023; Accepted 21 May 2023
Available online 8 June 2023

iteratively refined using a bundle adjustment (often a self-calibrating bundle adjustment). The inter-relationship, or model, between all of the locations, orientations and other parameters for all the images in the so-called *bundle* is sometimes known as the *photogrammetric model* (previously better known as the *stereo[scopic] model*). The quality of this refined photogrammetric model in turn influences the quality of the output 3D model (often generated by means of subsequent *dense image matching*). In order to assess the quality of (that is, to *validate)* the photogrammetric model it necessary to use independent measures.

In some cases, multiple cameras can be "posed" to view the target simultaneously as part of a "rig". Such rigs commonly have well defined "as-built" *a priori* estimates of interior and exterior orientation, which can be further refined through calibration, but compared to the use of a single COTS camera or phone they can be prohibitively expensive. There are many studies that have investigated the importance of control on photogrammetric models, using a single camera, with metre to kilometre extents, sometimes known as mega-scale (Agüera-Vega et al., 2017; James et al., 2017a, 2017b; Sapirstein and Murray 2017; Oniga et al., 2018; Sanz-Ablanedo et al., 2018). The same techniques cannot always be applied to smaller-scale digitisations due to inherent limitations of the control methods (e.g. size, range) and therefore different methods are needed.

This paper considers the use of photogrammetry for centimetre extent objects, specifically to look at any surface markings (e.g. toolmarks on bones, percussive marks on flint) (building upon work by Maté González et al., 2015, 2017, 2018; Yravedra et al., 2017; Barreau et al., 2022). In these types of applications, it is important to achieve control with $\leq$1 mm error, as the magnitude of the acceptable error will be related to the size of the object. Therefore, the focus of this research is to create and evaluate a simple, accessible, and systematic method of using 3D printed cradles to implement robust 3D control that can be used for the photogrammetric recording of small objects with COTS camera equipment.

2.1. 3D control for photogrammetry

The development of Structure-from-Motion, Multi-View Stereo (SfM-MVS) photogrammetry has allowed for more freedom in image capture, as the constraints for *a priori* camera parameters are more relaxed (Westoby et al., 2012). Some SfM software can perform photogrammetric reconstruction with minimal or no user intervention which whilst attractive to a busy user, can create products that are overly reliant on the automation provided by SfM and that do not benefit from the use of bespoke tie points (conjugate points identifiable by the user), which could otherwise improve the initial exterior orientation. In some cases, a scaled product may be required, for which a 2D target or scale bar is introduced if a photogrammetric rig cannot be used. Control points (CPs), that is identifiable points (preferably conjugant) in images with *a priori* 2D or 3D coordinates, are also an alternative. CPs have a known relative or absolute location and can be considered superior to scale bars in that they can be used to add not just scale but also orientation (requiring minimum three points) and spatial location to a model (Wolf et al., 2014; Linder 2016; Historic England, 2017).

Overall, in photogrammetric applications, it is optimal to have control spatially distributed as evenly as possible in all three dimensions (x, y, and z) in order to have a more robust bundle adjustment (Wolf et al., 2014; Historic England, 2017). If the control is spatially clustered, it may cause the bundle adjustment to be focussed on finding the best fit in just a small area, rather than across the entire surface to be reconstructed. CP locations can be with reference to a real-world Coordinate Reference System (CRS) which are then known as ground control points (GCPs) and result in a geo-referenced model with absolute exterior orientation (McCarthy 2014; Linder 2016). In other instances, CPs that will allow for scaling with arbitrary coordinates (also known as local coordinates) may be sufficient. When discussing properties and issues that can be associated with both CPs and GCPs, they can be indicated as [G]CPs. Where there is an abundance of [G]CPs a subset (ideally half) may be excluded from the bundle-adjustment for use in validation (Kasser and Egels, 2002, p155). In such cases these excluded points are known as check points (ChP) and the residual distances (either in 2D or 3D) between their *a priori* locations and their estimated locations in the photogrammetric model can be used to provide statistics for errors in said bundle-adjustment.

The use of 3D control for large-scale archaeological photogrammetric studies is commonplace often using artificial targets or existing, *in situ* identifiable features as the "targets" to provide 2D or 3D geo-referenced coordinates which are surveyed in through methods such as Global Navigation Satellite Systems (GNSS) and Total Station Theodolites (TST) (e.g. Chandler et al., 2007; Verhoeven 2011; AL-Ruzouq 2012; Verhoeven et al., 2012; Núñez et al., 2013; Olson et al., 2013; Sapirstein 2016; Agüera-Vega et al., 2017, Historic England, 2017). Often, using such equipment is physically impractical and their range or levels of precision are not appropriate for small objects. Macro- and meso-scale photogrammetry commonly apply 2D control through methods such as targets with known distances between, scale bars, or manufactured frames (e.g. Chandler et al., 2007; Abd Elbasit et al., 2009; Falkingham 2012; McQuaid et al., 2013; Gallo et al., 2014; Mallison and Wings 2014; Maté González et al., 2015; Porter et al., 2016; Rodríguez-Martín et al., 2016; Clini et al., 2016; Gajski et al., 2016; Historic England, 2017; Sapirstein 2018; Zawieska et al., 2019). In these situations, the targets can be distributed across the model, however there can be a lack of height differences of the control points so if working with an object that is tall or with variable height, a wider distribution of z-values will result in more robust control and a better model.

2.2. Accuracy and error in photogrammetry

In any methodological study involving metric values, measures such as accuracy, precision, reliability, and error are important for the purpose of validation (Fryer et al., 2007). Accuracy is how close the measured value is to the true one (otherwise known as *reference*), quantified as a statistic of the *differences* (Δ, more properly known as *residuals* or *residual errors*) (Wolf et al., 2014 p.495) and precision is how close repeated measured of a value are (Opitz, 2013; Wolf et al., 2014; Granshaw, 2016). Although reliability is similar to precision, it focuses on whether an instrument is interpreted consistently in different conditions (Field, 2009). As noted by Sapirstein (2018), all of these values improve with the use of [G]CP in photogrammetric modelling. Wolf et al. (2014) consider the various sources of residual error as including:

- *Gross error* (such as *user error*)
- *Systematic error* (such as mis-calibrated equipment)
- *Random error* (which is unavoidable and unpredictable).

Elements of industry concerned with the manufacture of precision machined components (for instance for aerospace or civil engineering) have often relied upon independent measurement of 3D coordinates or surfaces, or discrete points on an object's surface by means of servo driven pressure-sensitive probes, in a process known as [tactile] probing. The resulting coordinates are used to calculate residual errors relative to the original design. However, tactile probing has also been employed in as a means of validating photogrammetric models, as well as output 3D models, in close-range photogrammetry, the latter being a more cost-effective approach. Such probes can either be independent or integrated with the camera, which itself often has *a priori* interior and exterior orientation (Luhmann et al., 2013, pp404-405). Tactile probing would represent a useful means of validation the COTS approach presented here, were it not the size, weight and expense of the equipment being prohibitive for the applications we envisage.

In their recent meta-analysis on photogrammetry of human remains, Lussu and Marini (2020) found that of the studies that reported accuracy

of output 3D models (a total of seven, all having digitised crania or vertebrae) all had an accuracy of <5 mm, with some reporting <1 mm. Of these, some compared the photogrammetric models to 3D models created by other modalities (Lussu and Marini, 2020). Although this is informative, it is not the same as comparisons with independent measures, in terms of accuracy and error. Some studies compared their measurements to manual osteometry. For example, Morgan et al. (2019) found when measuring skulls, they had less than 2 mm mean difference between manual measurements and measurements from output 3D models. Among the range of setting configurations that they analysed; the best performing models had errors of less than 0.5 mm. In a similar 2022 study, Lauria et al. found a mean scale error of less than 0.2 mm when comparing manual craniometric measurements with digital ones from a photogrammetric model.

Other studies (for example Maté González et al., 2015) have attempted to validate either their photogrammetric models or output 3D models using residual errors observed with reference to a conventional scale bar or CP already used for either scaling or adjustment (that is to say, self-calibrating bundle adjustment). These generally report very high levels of accuracy and low levels of error, which is to be expected given no truly independent measures have been employed. Sapirstein (2018) employed an approach where a camera, pre-calibrated using a 2D field of coded targets, was used to photograph an object with both the same field of targets and a calibrated scale bar within the field-of-view. Accuracy was accessed using residual errors in measured distances (expressed as ratios) with reference to the target field and bar. This process was repeated for different cameras and settings, resulting in a comprehensive repeatability study. Further, the scaling required between repeat output 3D models was used as an additional means of validation. Where CP to are used to refine single photogrammetric models (that is to say, self-calibrating bundle adjustment of the interior and exterior orientation), and where repeat photography is not employed for repeatability studies, ChP may also be used as a truly independent measure of such by providing residual errors for use in validation. In contrast, measuring a scale bar to check for errors is somewhat analogous to measuring the CP rather than ChP in this situation.

3. Materials and methodology

3.1. Equipment

In this research a Nikon D5300 (DX format camera) and D810 (FX format camera) were (Nikon 2020a) paired with a 60 mm FX macro lens (DX-compatible) (Nikon 2020b). The specifications of the cameras, lens, and computer used are listed in (Tables S.1-S.3).

In deciding on how to create 3D control in the cradles, both the quality of the control and the accessibility of the method were important aspects which needed to be balanced. From the outset the intent was for the cradles to be created using additive manufacturing (more commonly

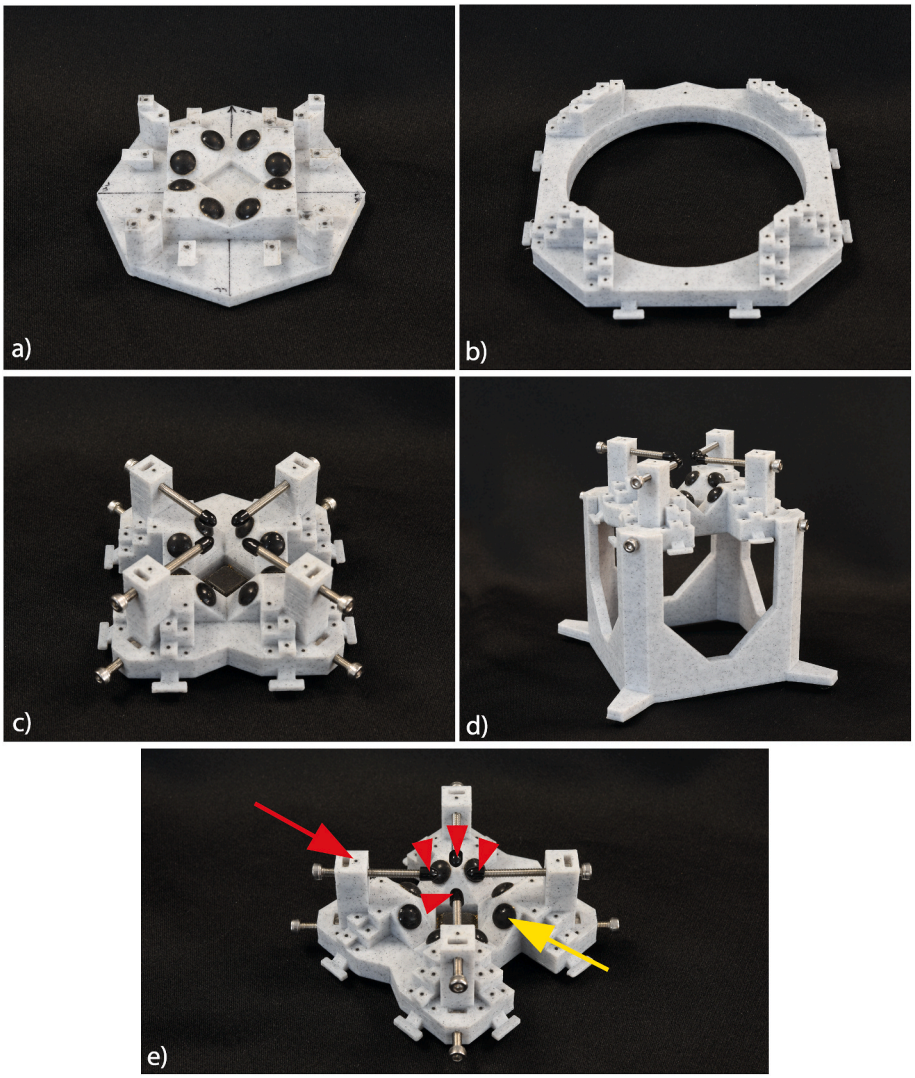

Fig. 1. The three cradles that were used for this project, a) the original cradle (OG), b) the cradle designed for larger objects (PH), c) the adaptations of the original (MK2), d) the stand for MK2 to allow more clearance of objects that would overhang, and e) an annotated version of MK2 with the control points (red arrow), gripping semi-spherical stickers (yellow arrow), and four-screw support mechanism (red arrowheads) highlighted. (For interpretation of the references to colour in this figure legend, the reader is referred to the Web version of this article.)

known as 3D printing) and these were used to add 3D control into the model (Fig. 1), such that they could be created repeatedly and inexpensively by anyone with access to a desktop consumer-grade machine (in this case an Ender-3 with heated bed) and inexpensive Poly Lactic Acid (PLA) filament. This approach also permitted rapid prototyping and iterative redesign.

Three "control cradles" were designed in the freeware Computer Aided Design (CAD) software Trimble™ (previously Google™) Sketchup. CAD files were "sliced" into Sterolithography/Standard Triangle Language/Standard Tessellation Language (STL) format using Ultimaker™ Cura for 3D printing.

The first consideration of the CAD design was the need to hold an object firmly, such that it would not move (either in terms of translation or rotation), without damaging it. Thus, there needed to be sufficient room to add self-adhesive rubber pads, to use as a "bed" for the object, as well as the ability to secure the object with either 1) rubber bands fixed around hooks; and/or 2) horizontal, adjustable screws with rubber-end caps. We found that adding wedges between the cradles and target objects increased the latter's security and visibility. Therefore, bespoke wedges were also designed in CAD and 3D printed, such that their shape and dimensions would fit within some of our cradle designs. In one case, a 3D printed stand was also designed to fit a cradle, such that it could be raised to accommodate objects with awkward shapes.

The second consideration was the fixed points with pre-defined (as-designed) co-ordinates. Points needed to be of sufficient number and distribution that 1) approximately half could be used for control and the remainder as check points; 2) the majority could be imaged without also occluding significant parts of the target object (any parts of the cradle that were obscured from one viewpoint were designed to be visible from at least two other viewpoints); and 3) they were separated in elevation (Z axis), as well as horizontally (X and Y axes), to create true 3D control. The latter necessitated the use of "towers" to create elevated platforms for points. The control cradles were designed to be symmetrical to make the alignment with the camera easier.

Points also needed to contrast with their surroundings and have a consistent diameter (such that their centre could be readily, reliably, and repeatedly identified by the user). At the millimetre scales required this could not be accomplished with sufficient accuracy using ink or paint. Therefore, the decision was made to create holes in the 3D design which could accommodate a separate length of black material of consistent diameter, which could be glued in place and them sliced off to be flush with the surrounding surface. The chosen material was 1 mm diameter black rubber gasket, fixed in place using cyanoacrylate (liquid) adhesive and sliced using a scalpel. Although some photogrammetric software has the ability to automatically detect certain patterns within a control point marker, this type of control point was not used in this study for two major reasons. The first was that the scale of the entire model was too small to fit the desired number of control points if they were printed with a pattern. The second was that the cradles were designed to be accessible and therefore the decision was made to avoid adding anything that would link them solely to a specific software.

The third consideration was ease of production. The design needed a flat base (to which adhesive rubber feet could be stuck) so as to be stable on a desk or other horizontal surface used during photography. However, this had to have few-or-no angulate corners which might otherwise promote the cradle separating from the bed of the 3D printer, even when using a headed bed and/or brim and raft structures.

A grey filament with black flecks (currently only available in PLA) produced a surface with even but randomly distributed specks. These resulted in the automated identification of more conjugate points between photographs and therefore a more robust initial photogrammetric model (as illustrated in the dense point cloud in Fig. 4).

Our iterative rapid prototyping and redesign resulted in the cradles and accessories illustrated in Fig. 1. These cradles were known as "OG", "MK2", and "PH" and they all were designed for slightly different geometries of bone. OG and MK2 have a series of associated wedges in order to angle the object when required.

The first, bespoke control cradle (OG, 20 CP[12 Cp, 8 ChP]) was designed in Sketchup, sliced using Cura, and printed on an Ender-3 (Fig. 1a). It was designed for the object to rest in the middle and be fixed in place using elastic bands. As described, each of these control points was 1 mm in diameter and when the marker identifying the cutmark was manually placed in Agisoft Metashape™, it was placed as centrally as possible.

A second cradle (MK2, 26 CP, 26 ChP) was designed based on what was learned using the first (Fig. 1c and d). This version had a deeper central V in order to aid objects to be held vertically. It also included a system of adjustable nuts and bolts that could be used to secure an object in place without requiring elastic bands, as the latter would often occlude part of a surface. Additional CP were added such that half could then be used as ChP. A third, additional cradle (PH, 30 CP, 30 ChP) was created for objects that would not readily rest within the existing cradle whilst still maintaining proximity of the target area to the CP. It was designed to sit on top of and surrounding the subject (Fig. 1b).

Another major benefit of these control cradles is that if placed on an unmarked background, the control cradle and object can be rotated together and the camera left stationary since the control points will stay in the same place relative to the bone with no other confounding marks. This helped reduce image capture time. Subsequently, additional wedges and attachments were designed and printed for both cradles in order to them more universal (Fig. 2).

All cradles and wedges are available for other researchers to use or modify to their specifications and print at https://www.thingiverse.com/thing:5376182.

3.2. Case study

The efficacy of the 3D control built into the bespoke 3D printed cradles was tested through their use in the creation of photogrammetric models of bone fragments (<10 cm) and the measurement of cutmarks on them. The bones are from a mass grave excavated in South Dorset in 2009.where 52 individuals were discovered dating to the late 10th century CE. Chemical analysis has revealed that they are non-local, originating from parts of Scandinavia, and the collection has been commonly referred to as the "Weymouth Ridgeway Vikings" (Chenery et al., 2014; Loe et al., 2014). The bones display repeated examples of sharp force injuries (Tamminen et al., 2019, 2023). The cutmarks range in width from less than 1 mm wide to 50 mm, whilst the length is equally diverse, spanning from approximately 2 mm–70 mm (Loe et al., 2014). In osteoarchaeology and forensic anthropology, cutmarks such as these can provide valuable information about the mechanism of injury and the digitisation of such injuries can increase the types of analysis that are performed whilst preserving the bone itself (Smith and Brickley 2004; Cohen et al., 2012; Symes et al., 2012; Harten-Buga et al., 2018; Maté-González et al., 2018; Vazzana et al., 2018; Courtenay et al., 2019; Barreau et al., 2022).

3.3. Methods

The cut bones selected to create the photogrammetric models for this case study were divided into two categories based on geometry; incised cutmarks which have left an impression in the bone and shaved cutmarks which have bisected the bone. A total of ten of each were selected for this study and various manual and photogrammetric measurements were taken; length, width, wall heights; and opening angle (the former two only possible on shaved cutmarks). All manual and photogrammetric measurements were taken three times and averaged before being repeated once, two to three days later, to analyse intra-observer error.

To collect the images to create the 3D models, the bones, were placed in the centre of each of the three different control cradles and secured using the cradle screws or elastic bands (See Fig. 3). For each control cradle-object set up the complex was then centred on a flat surface with

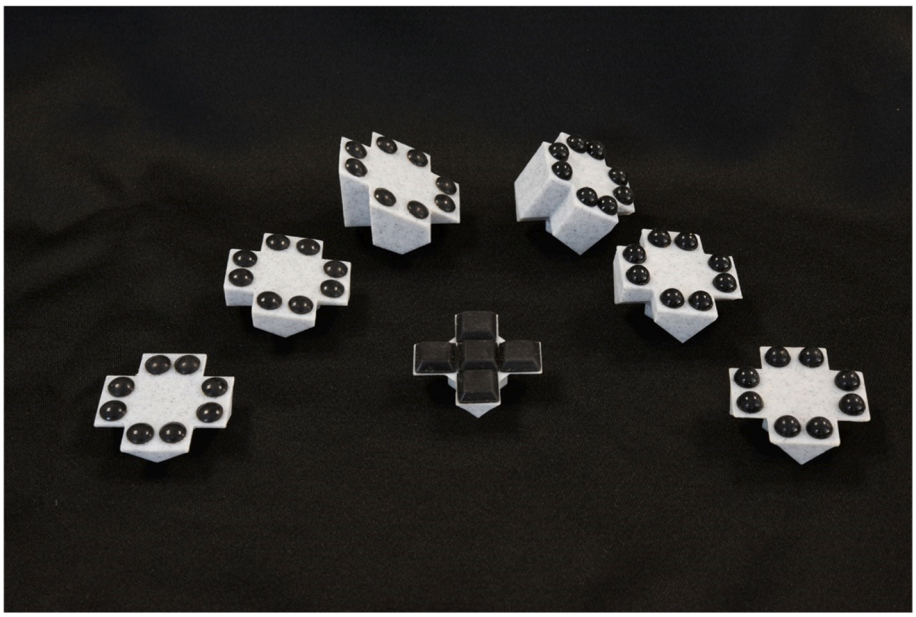

Fig. 2. The wedges that were designed and printed for cradles OG (left) and MK2 (right) with angles of 30°, 10°, and 0° (back to front).

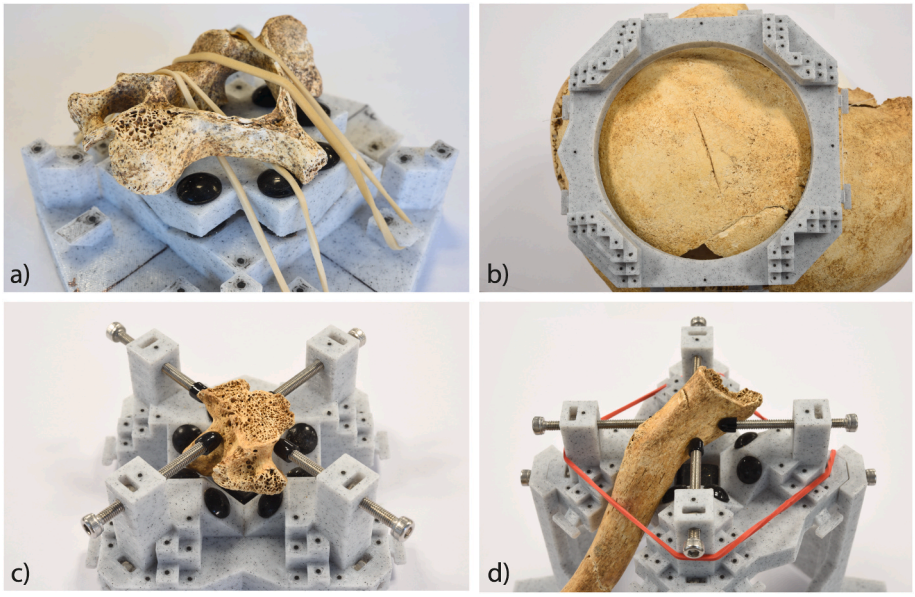

Fig. 3. Examples of images with the bones secured in the cradles with a) showing OG and a wedge, b) showing PH, c) showing MK2, and d) showing MK2 and its associated stand.

a neutral background and lighting which was as diffuse and non-directional as possible (so as to prevent either over-exposed or shaded areas, which would otherwise reduce the number of matched conjugate points).

The photographic capture strategy used for all of the cradle-object set ups was designed based on giving maximum coverage whilst remaining efficient. A "Union Jack" pattern was chosen as it allowed for all angles to be covered with sufficient overlap for the software to be able to effectively create a model (Fig. 4). A total of 17 images were taken for each cutmark and the camera was angled at 22.5°, 45°, and 90° for the images.

All pictures were shot in RAW (.NEF for Nikon) and transformed into 16-bit greyscale TIFFs to avoid the loss of data. After iterative testing to determine the best methods for this type of subject, the models were processed using the workflow seen in Fig. 5. In general, the methods of Maté-González et al. (2015, 2017, 2018) and Mallison and Wings (2014) were used as a starting point for the workflow created here. Adaptations were made based on various sources such as Sapirstein (2018).

Images were imported into Agisoft Photoscan/Metashape and aligned on High. From there, the CP locations were imported and placed on their respective CPs to allow the model to be scaled. The model was Optimised and then edited using the Gradual Selection tool to ensure the best possible sparse point cloud. Once a second Optimisation was run, a dense point cloud was created, also on High with Depth Filtering Disabled. The latter was important in this study because the topographic changes of the cut marks could be very minute and therefore could be accidently removed during interpolation if Depth Filtering left on. Saving the point clouds as ASCII files (.txt) was the final step in creating the models (Fig. 6).

Subsequent analysis could be run on these point clouds in any

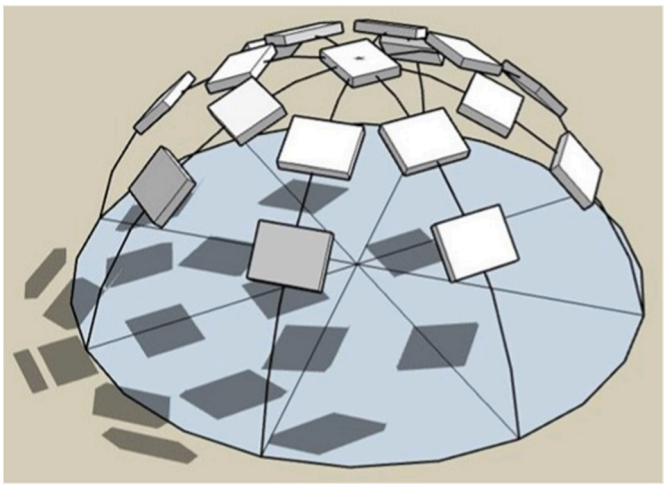

Fig. 4. The "Union Jack" image capture pattern that was used to photograph the objects in the cradles.

software that accepts that file format. In order to compare the measurements from digital models and manual methods, CloudCompare and ImageJ were used. Depending on the measurements required, ImageJ may not be required. In CloudCompare, the Point Picking tool is used to gather linear measurements or angles. Since measurements can only be taken between points, alternative software may be needed for angles where there is curvature. In those situations, the "Extract Sections" tool within Segmentation was used to extract a profile of the cutmark to examine from a "side-on" view. This viewpoint was then extracted as an image and imported into ImageJ to obtain the angle measurements required.

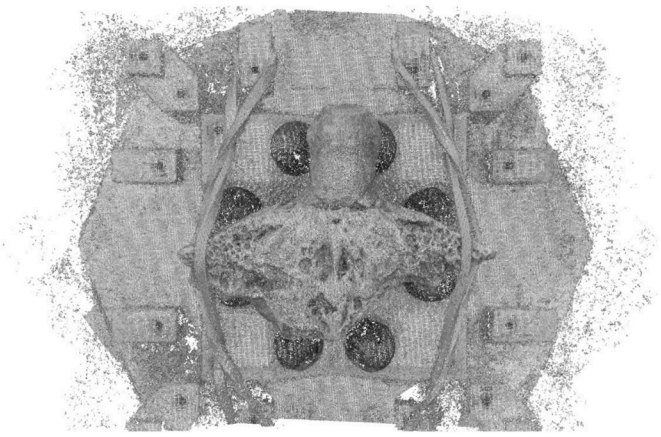

Fig. 6. An example of a dense point cloud created as one of the initial iterative tests to find the optimal workflow.

The models that were created were analysed in multiple ways using the error output from the Reference Pane in Metashape so as to investigate the quality of the differentcontrol cradles and their 3D outputs. The efficacy of the different cradles was investigated both with and without the inclusion of human-taken measurements. The CP and ChP error investigations dis not involve any manual measurements and do not involve the cutmarks to negate the impact of human-related error (See 3.3.1 and 3.3.2). Measurements were taken for the aspect that involved the comparisons of methods (manual vs digital; See 3.3.3).

3.3.1. Cradle quality: control point and check point error tests

CP and ChP error tests were undertaken to provide an independent check of the quality of the models. Three FX models were randomly

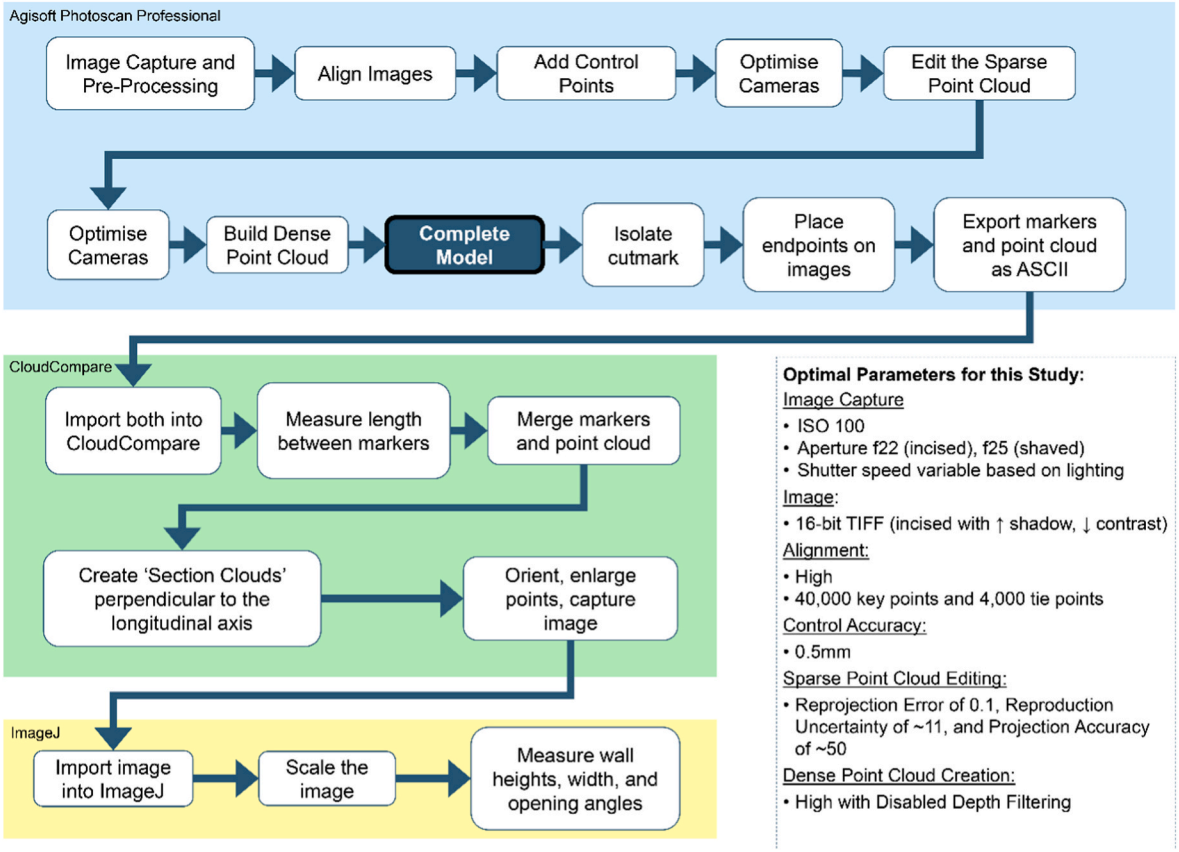

Fig. 5. The workflow used in this project to achieve the optimal results.

selected, one from each control cradle type. The two types of cutmarks, shaved and incised, were not differentiated for this portion. Cradles PH and MK2, both designed to have an equal number of CP and ChP, were investigated using a symmetrical pattern of each CPs and ChPs in order to check the accuracy and precision of the model. Although not designed with ChP in mind, cradle OG was also tested with twelve CP and eight ChP. This configuration was used to avoid leaving large gaps in control.

In all cases, the model was aligned, edited, and optimised (using a Self-Calibrating Bundle Adjustment) before the ChP were added, in order to deduce their error compared to the CP error. In this aspect of the analysis, no measurements were taken of the cutmarks because the focus was on the quality of the cradles rather than the accuracy of measurements. Descriptive statistics and normality tests were run on these errors for the chosen models before a Mann-Whitney *U* test was used for statistical comparison since not all datasets were considered normal and parametric according to the Shapiro-Wilk test.

3.3.2. *Cradle quality: systematic error tests*

The final aspect that was investigated was if there were correlations between the error and the value of each cradles' CPs. For each cradle, five FX models were randomly chosen to export the coordinates. The values of each x, y, and z were plotted against the absolute x, y, and z errors to see if the error was random (no correlation) or systematic (correlation). A Spearman's Rho was used for this.

3.3.3. *Models of the bones*

Also examined were intra-observer error and differences between methods of measurement (manual, DX photogrammetry, and FX photogrammetry). Length and width measurements were also taken on a subsample of the models created for the initial case study, using the DX and FX models, but analysing them separately. All manual measurements were taken with digital callipers (Mitutoyo CD-6" ASX). The two types of cutmarks were treated separately at this point (Study 1 involving incised cutmarks, Study 2 involving shaved ones), due to the geometric differences, with ten examples of cutmarks for each category.

The same measurements were taken using digital callipers as well since this is the conventional way of gathering such measurements (e.g. Fiorato et al., 2000; Loe et al., 2014; Giuffra et al., 2015). Intra-observer error was checked by repeating the digital and manual measurements a week later and doing a non-parametric repeated measures test in order to see if the measurements were statistically similar. Both Wilcoxon Signed Rank Test and the Sign Test were used. The former was found to be influenced more by the small sample size than other variables, therefore the latter was run as well. Boxplots were also used to visually compare the medians and interquartile ranges.

The different measurement methods, including DX compared to FX, were also compared to determine if the values that were obtained were statistically similar. The Friedman Test, the Wilcoxon Signed Rank Test, and the Sign Test were used for this analysis, depending on how many variables were being compared.

4. Results

All models created with the control cradles were successful and of consistently good quality, both visually and metrically. The summary statistics, normality, and statistical differences for the CP and ChP values and errors for all three cradles are presented in Tables 1 and 2 The former displays the overall errors with the latter showing the error broken down into constituent x, y, and z parts. These were used to examine if there were significant differences between the errors in the two sets of points and no statistically significant difference was found.

Additionally, the errors and values of each CP were examined for a subset of models to determine if there was systematic error within each cradle itself. Visually, when examining the scatterplot of z-values and z-errors (especially MK2), there appeared to be a relationship, however, this was statistically non-significant though may still need further investigating with a larger dataset (see supplemental file, Table S.4). MK2 was the tallest of the three cradles and therefore had a much wider range of z-values than the other cradles. OG did show a significant relationship in the z-direction but the relationship is not strong enough to be a problem. The error was still considered to be small despite this. Statistical significance was seen in some of the x and y-values and errors, but all the relationships were weak and are not thought to confound the results.

Length, width, wall height, and opening angle measurements (the latter two where applicable only) were taken using the 3D models (FX and DX cameras) and manual methods in order to investigate whether the measurements obtained from the 3D models were statistically different than those through conventional methods (descriptive statistics within Table 3). Due to the small sample sizes with tied values, the Sign test was prioritised for the intra-observer error. These were all found to be statistically non-significant and no visual differences were seen in boxplots displaying median and inter-quartile range (Table 4, Figure S1-2). All results were found to have statistical similarity, thus leading to the conclusion that the measurements taken from the photogrammetric models and those manually obtained using callipers were virtually identical. When comparing DX, FX, and manual measurements using a Friedman Test for both studies, p-values of 0.301–0.723 were seen. When comparing the same pair-wise, p-values of 0.114–0.906 (Wilcoxon Signed Ranks Test) and 0.109 to 1.000 (Sign Test). A Bonferroni correction was implemented where required, and because the values were non-significant, this did not affect the results. Full tables are found in the supplemental file (Tables S.5-S.7).

5. Discussion

The results show that 3D control cradles create good quality models with easily identifiable surface alterations (cutmarks) from which precise measurements can be taken. The values obtained are not statistically different than manual measurements which are the most common method of analysing the type of sample used in this study. This was similar to what was found by Maté-González et al. (2017, 2018). The cradles are adaptable and can be printed to the specifications of the

Table 1
The summary statistics and Shapiro-Wilk results for the overall error (in mm) in the check and control points with significant values in bold and the p values in parentheses.

	OG (N_{CP} = 12, N_{ChP} = 8)		MK2 (N_{CP} = 26,N_{ChP} = 26)		PH (N_{CP} = 30, N_{ChP} = 30)	
	Control	Check	Control	Check	Control	Check
Mean	0.081	0.078	0.157	0.158	0.328	0.306
SD	0.036	0.040	0.084	0.105	0.123	0.102
SE of Mean	0.010	0.014	0.017	0.021	0.022	0.019
Median	0.073	0.092	0.138	0.137	0.355	0.313
IQR	0.024	0.068	0.064	0.086	0.175	0.089
Range	0.114	0.109	0.394	0.458	0.560	0.490
Shapiro-Wilk	**0.810 (0.012)**	0.895 (0.261)	**0.833 (0.001)**	**0.784 (<0.001)**	0.963 (0.360)	0.931 (0.053)
Mann-Whitney U	48.000 (1.000)		319.000 (0.728)		378.500 (0.290)	

Table 2
The summary statistics and Shapiro-Wilk results for the error (in mm) in the check and control points with significant values in bold and the p values in parentheses broken down into x, y, and z components for each cradle.

		x		y		z	
		Control	Check	Control	Check	Control	Check
OG ($N_{CP} = 12$ $N_{ChP} = 8$)	Mean	0.039	0.028	0.038	0.039	0.050	0.051
	SD	0.023	0.021	0.030	0.031	0.031	0.039
	SE of Mean	0.007	0.007	0.009	0.011	0.009	0.014
	Median	0.037	0.024	0.029	0.039	0.047	0.038
	IQR	0.039	0.019	0.038	0.061	0.038	0.062
	Range	0.072	0.071	0.107	0.072	0.114	0.114
	Shapiro-Wilk	0.957 (0.746)	0.863 (0.130)	0.894 (0.132)	0.853 (0.103)	0.915 (0.246)	0.903 (0.309)
	Mann-Whitney U	32.000 (0.217)		46.000 (0.877)		44.500 (0.787)	
MK2 ($N_{CP} = 26$ $N_{ChP} = 26$)	Mean	0.062	0.092	0.069	0.066	0.109	0.081
	SD	0.046	0.082	0.050	0.052	0.081	0.085
	SE of Mean	0.009	0.016	0.010	0.010	0.016	0.017
	Median	0.042	0.063	0.053	0.055	0.108	0.056
	IQR	0.065	0.087	0.080	0.056	0.082	0.069
	Range	0.174	0.343	0.175	0.221	0.353	0.368
	Shapiro-Wilk (W)	**0.907 (0.022)**	**0.834 (0.001)**	0.942 (0.151)	**0.834 (0.001)**	**0.847 (0.001)**	**0.770 (<0.001)**
	Mann-Whitney U	273.000 (0.234)		310.500 (0.615)		232.000 (0.052)	
PH ($N_{CP} = 30$ $N_{ChP} = 30$)	Mean	0.195	0.195	0.166	0.134	0.138	0.120
	SD	0.114	0.116	0.130	0.116	0.095	0.094
	SE of Mean	0.021	0.021	0.024	0.021	0.017	0.017
	Median	0.181	0.161	0.132	0.102	0.130	0.103
	IQR	0.195	0.172	0.186	0.158	0.118	0.139
	Range	0.444	0.435	0.447	0.472	0.415	0.396
	Shapiro-Wilk	0.975 (0.681)	0.955 (0.236)	**0.880 (0.003)**	**0.892 (0.005)**	0.935 (0.068)	**0.925 (0.037)**
	Mann-Whitney U	433.500 (0.807)		386.500 (0.348)		397.000 (0.433)	

Table 3
The descriptive statistics for Tests 1 and 2 from Study 2 with length and width measurements in mm.

Measurement	Statistic	DX		FX		Manual	
		Test 1	Test 2	Test 1	Test 2	Test 1	Test 2
	N	10	10	10	10	10	10
Length	Mean	18.680	18.677	18.737	18.745	18.549	18.691
	SE of Mean	2.836	2.838	2.803	2.813	2.831	2.802
	Median	16.365	16.205	16.380	16.245	15.775	15.755
	25%ile	13.480	13.525	13.613	13.630	13.618	13.608
	75%ile	22.450	22.470	22.448	22.565	22.473	22.575
	IQR	8.970	8.945	8.835	8.935	8.855	8.968
Width	Mean	9.319	9.287	9.337	9.334	9.444	9.360
	SE of Mean	1.328	1.331	1.317	1.322	1.333	1.339
	Median	8.675	8.715	8.655	8.680	8.770	8.695
	25%ile	6.043	5.983	6.195	6.158	6.138	6.175
	75%ile	10.853	10.785	10.815	10.828	10.860	10.883
	IQR	4.810	4.803	4.620	4.670	4.723	4.708

objects under investigation. They are also easy to set up and use. The cradle proved to be very versatile and when applied to a much larger collection (requiring approximately 450 models, all were successful and about two-thirds of those were created with the original cradle and two wedges (Tamminen et al., 2019; Tamminen 2022). Therefore, this method of adding full 3D control to small objects is a large step forward in creating high quality models which can be used for metric analysis.

5.1. The creation of control cradles

When deciding on how to create 3D control, both the quality of the control and the accessibility of the method were important aspects which needed to be balanced. Overall, the use of 3D printing was decided to be the best way to make something that was bespoke. How this decision would impact the accessibility of this method was considered thoroughly as it requires access to a 3D printer. Rapid prototyping services are now readily available. Costs are impacted by the material type and object size. Therefore, for small items like the control cradles, this method has the potential to be a low-expense option to obtain a bespoke and highly reusable piece of equipment which would incorporate control for instances that the interior and exterior camera orientations and locations were not known.

5.2. The comparative measurements

The results from the case study show that the measurements from the point clouds are statistically similar to the measurements that were taken manually off the bone, which is generally the conventional manner of measuring. This indicates that the digital measurements are able to be used in place of the manual ones without introducing additional error.

The models created by the FX and DX cameras were not found to have any differences between them and therefore the method is shown to be fairly robust to changes in the quality of the camera which makes this technique more widely accessible. After this was established, the FX camera was primarily used.

Table 4
The Intra-observer error results for the Wilcoxon Signed Rank and the Sign Test for the length, width, wall heights, and opening angle in Project Study 1 and 2.

Project Study	Measurement	Statistic	DX	FX	Manual
PS1	Length	Z	-0.153[c]	-0.255[c]	-0.561[b]
		Wilx Sig.*	0.878	0.799	0.575
		Sign Exact Sig.	0.754[#]	1.000[#]	1.000[#]
	Width	Z	-0.051[b]	-1.588[b]	-0.210[b]
		Wilx Sig.*	0.959	0.112	0.833
		Sign Exact Sig.	0.754[#]	0.109[#]	0.727[#]
	Wall Height 1	Z	-1.785[c]	-1.071[c]	–
		Wilx Sig.*	0.074	0.284	–
		Sign Exact Sig.	0.754[#]	0.754[#]	–
	Wall Height 2	Z	-0.652[c]	-1.009[c]	–
		Wilx Sig.*	0.514	0.313	–
		Sign Exact Sig.	1.000[#]	0.508[#]	–
	Opening Angle	Z	-0.051[b]	-1.478[c]	–
		Wilx Sig.*	0.959	0.139	–
		Sign Exact Sig.	1.000[#]	0.109[#]	–
PS2	Length	Z	-0.102[c]	-0.474[c]	-1.888[c]
		Wilx Sig.*	0.919	0.635	0.059
		Sign Exact Sig.	1.000[#]	1.000[#]	0.109[#]
	Width	Z	-2.094[b]	-2.094[b]	-0.255[b]
		Wilx Sig.*	0.036	0.779	0.799
		Sign Exact Sig.	0.180[#]	1.000[#]	0.754[#]

*Asymp. Sig. (2-tailed).
#Binomial distribution used.
[a]. Wilcoxon Signed Ranks Test.
[b] Based on positive ranks.
[c] Based on negative ranks; Test 2 - Test 1.

5.3. The control points

Overall, the errors that were found for all the CP were considered acceptably low for the current purpose. The error was the lowest in the OG cradle (~0.07–0.1 mm), slightly higher in MK2 (~0.17–0.19 mm), and highest in PH (~0.3 mm). The latter is understandable as the size of the cradle meant that the images had to be taken from further away. This is also reflected in the lowest pixel error in these photosets.

Although not statistically significant, the correlation between z-value and z-error should be further explored to determine the cause and any methods to mitigate for it. Within the remit of this study, the errors produced were still considered acceptably small. The statistical significance of some of the other correlations was unexpected, but given both the appearance of the graphs and the weakness of the relationship, these are not thought to be demonstrative to systematic errors that need attention.

5.4. The check points

In all cradles, the errors that were found were statistically similar to and followed the same pattern as those found in the CP, thus supporting the findings from the measurements that this photographic strategy with the control cradles results in a model of good photogrammetric quality. The overall error as well as the absolute x, y, and z-error were all examined in the same manner and presented the same results. Therefore, this shows robust 3D control is provided by the cradles and they are fit for purpose.

5.5. The use of control cradles

The control cradles were found to be very useful and simple to work with; they helped reduce capture time and increased the consistency with which the images were taken. They are lightweight and easily transportable. The models that were created of the cutmarks were very detailed (Fig. 7). With each attachment to the control cradles, more bones can be accommodated, however, it is a challenge to make a single cradle that fits all bones in a collection appropriately. This does add to the time and cost invested when creating a cradle, but as demonstrated by this study, itis seen to be very versatile even with minimal attachments. Additionally, if objects to be digitised are significantly different shape, the designs published alongside this paper should allow further bespoke adaptation to accept such. Extra set-up time must be added for the virtual placement of markers on the CP, but that is not due to a control cradles but rather the use of control in general and thus will always be present. This time may also be off-set by the decreased capture time, which resulted in overall similar timings to what was described by Sapirstein (2018) (see supplemental file, Table S.8).

As the use of photogrammetry increases, especially by users who may not have access to the highest-specification equipment, it is important to determine the full capabilities and limitations of current methods to avoid creating poor models that are not fit for purpose in the future. When designing equipment and methodologies, it is ideal to compare the results achieved against a "true" measurement of an object using a "gold standard" (Versi 1992; Walsh 2018). Within this study, the comparison to manual measurements was deemed an acceptable comparison since that is the most common “low-tech” metric method of data capture on human skeletons.

Intra-observer reliability has been demonstrated, but inter-observer error was beyond the scope of this study. Therefore, this should be investigated across users with various levels of experience both at creating models and analysis to determine if this combination of control and methodology can be used at all levels of skill. Additionally, and importantly, there is room for further exploration into the changes that

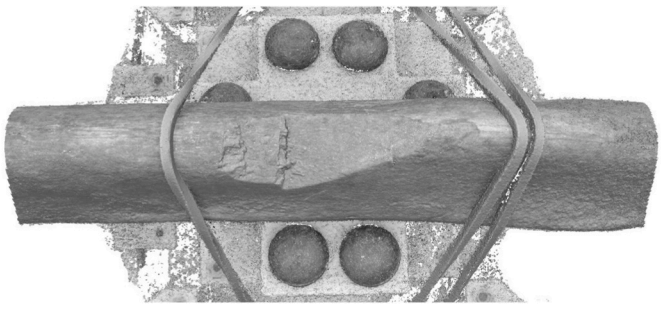

Fig. 7. An example of a dense point cloud of a cutmark created using the OG cradle.

are seen in the models with different cameras and software packages, especially with freeware.

5.6. The digital benefit

In this manuscript, we have provided a method for using an independent 3D system to check the accuracy and error of, or validate, the model. CPs were used to refine models, whilst the unused black markers on the cradles (the ChPs) were used as independent measures, without the influence of the CPs or human measurement error (the latter of which would have been present had the quality checks solely relied on the cutmark measurements). The levels of accuracy that were found were similar to those in Lauria et al. (2022) and Morgan et al. (2019), both of which compared a range of 2D manual osteometric measurements to equivalent measurements on their 3D models.

Although the use of independent measurements to validate models inherently provides higher error and lower accuracy than some of the methods of analysis mentioned at the beginning of this paper, the independent validation better reflects the quality of the model.

The digitisation of archaeological sites and artefacts continues to become more common (Magnani et al., 2020). The ability to digitise at a macro scale with high accuracy and precision is beneficial for recording, preservation, and research. Digital models allow for the mathematical comparison of different surface or objects, something that cannot be done as easily using the actual artefacts. This is a method of preserving the artefact for future study as well, allowing for continual study without damaging the original. It also allows for replicable studies, even if they are "destructive". The 3D digitisation of objects, such as cutmarks, can also lead to new information being uncovered about a collection (Tamminen et al., 2023; See Errickson et al., 2012 for further discussion on the benefits of digitising osteological remains).

6. Conclusion

Overall, photogrammetry is an effective, ever-evolving technique and the capabilities and limitations especially for metric analysis are still under investigation. Within this paper, the design of a range of 3D control cradles are presented with the files required to modify and 3D print to whatever specifications are required. These cradles provide 3D control for close-range models when it cannot be established through *a priori* knowledge of the interior and exterior orientation of the camera alone.

COTS personal 3D printing is becoming more commonplace and inexpensive and the hope is that this design will be able to be used in tandem with photogrammetry to allow for a more accessible method of 3D digitisation. The results from this study have shown that these control cradles work efficiently and produce good quality results when coupled with an effective methodology. The cradles evaluated here are easy to use and therefore are considered an asset to use in close-range photogrammetry that requires high metric quality.

Author statement

All authors significantly contributed to this work.

HMT: Conceptualisation, Methodology, Data Capture, Data Analysis, Visualisation, Writing – original draft, Writing – review & editing.

KW: Writing – original draft, Writing – review & editing, Supervision.

MJS: Conceptualisation, Writing – original draft, Writing – review & editing, Supervision.

ALJF: Conceptualisation, Methodology, Data Analysis, Writing – original draft, Writing – review & editing, Supervision.

Declaration of competing interest

We have no conflicts of interest to disclose. This work was part of the lead author's doctoral research, funded jointly by Bournemouth University and the Dorset Museum.

Acknowledgements

The authors would like to thank the Dorset Museum, Dr Jon Murden, and Miss Elizabeth Selby for providing the opportunity to analyse the case study collection. Additional thanks go to the original excavators and examiners of the collection, Oxford Archaeology, and the Human Osteology Team at Bournemouth University. We thank the reviewer for their thorough comments which have improved this paper and the editor for their help along the way.

This work has been part of a joint-funded PhD between Bournemouth University and the Dorset Museum undertaken by the lead author. This research did not receive any other specific grants from funding agencies in the public, commercial, or non-for profit sectors.

Appendix A. Supplementary data

Supplementary data to this article can be found online at https://doi.org/10.1016/j.daach.2023.e00273.

References

Abd Elbasit, M.A.M., Anyoji, H., Yasuda, H., Yanamoto, S., 2009. Potential of low cost close-range photogrammetry system in soil microtopography quantification. Hydrol. Process. 23, 1408–1417. https://doi.org/10.1002/hyp.7263.

Agüera-Vega, F., Carvajal-Ramírez, F., Martínez-Carricondo, P., 2017. Assessment of photogrammetric mapping accuracy based on variation ground control points number using unmanned aerial vehicle. Measurement 98, 221–227. https://doi.org/10.1016/j.measurement.2016.12.002.

AL-Ruzouq, R., 2012. Photogrammetry for archaeological documentation and cultural heritage conservation. In: Carniero da Silva, D. (Ed.), Special Applications in Photogrammetry. InTech, Rijeka.

Ashton, N., Lewis, S.G., De Groote, I., Duffy, S.M., Bates, M., Bates, R., Hoare, P., Lewis, M., Parfitt, S.A., Peglar, S., Williams, C., Stringer, C., 2014. Hominin footprints from early pleistocene deposits at happisburgh, UK. PLoS One 9 (2), e88329, 1-13.

Barreau, J.-B., Gagnier, A., Gaugne, R., Marchand, G., Calvo Gómez, J., Gouranton, V., Colleter, R., 2022. Use of different digitization methods for the analysis of cut marks on the oldest bone found in Brittany (France). Appl. Sci. 12 (3) https://doi.org/10.3390/app12031381.

Bartzis, D., 2017. Towards reconstructing a Doric column in a virtual construction site. In: Aguilera, D., Georgopoulos, A., Kersten, T., Remondino, F., Stathopoulou, E. (Eds.), The International Archives of Photogrammetry, Remote Sensing and Spatial Information Sciences, Volume XLII-2/W3, vol. 2017. 3D virtual reconstruction and visualization of complex architectures, Nafplio, pp. 91–96. https://doi.org/10.5194/isprs-archives-XLII-2-W3-91-2017, 1-3 March 2017.

Bleed, P., Douglass, M., Sumner, A., Behrendt, M., Mackay, A., 2017. Photogrammetrical assessment of procedural patterns and sequential structure in "handaxe" manufacture: a case study along the Doring River of South Africa. Lithic Technol. 42 (1), 3–12. https://doi.org/10.1080/01977261.2016.1265205.

Bryan, P., Chandler, J.H., 2008. Cost-effective rock-art recording within a non-specialist environment. In: Chen, J., Jiang, J., Maas, H.-G. (Eds.), International Archives of the Photogrammetry, Remote Sensing and Spatial Information Sciences XXIst ISPRS Congress Technical Commission V. Beijing, pp. 259–264, 3-11 July 2008.

Cârlan, I., Dovleac, B., 2017. 3D modelling of Arutela Roman Castrum using close-range photogrammetry. Int. J. Conserv. Sci. 8 (1), 35–42.

Chandler, J.H., Bryan, P., Fryer, J.G., 2007. The development and application of a simple methodology for recording rock art using consumer-grade digital cameras. Photogramm. Rec. 22 (117), 10–21.

Chenery, C.A., Evans, J.A., Score, D., Boyle, A., Chenery, S.R., 2014. A boat load of Vikings?. Viking settlers of the North Atlantic: an isotopic approach. Journal of the North Atlantic. Special volume 7, 43–53.

Clini, P., Frapiccini, N., Mengoni, M., Nespeca, R., Ruggeri, L., 2016. SfM technique and focus stacking for digital documentation of archaeological artifacts. In: Halounova, L., Šafář, V., Remondino, F., Hodač, J., Pavelka, K., Shortis, M., Rinaudo, F., Scaioni, M., Boehm, J., Rieke-Zapp, D. (Eds.), The International Archives of the Photogrammetry, Remote Sensing & Spatial Information Sciences, Volume XLI-B5. 2016 XXIII ISPRS congress, Prague, pp. 229–236. https://doi.org/10.5194/isprsarchives-XLI-B5-229-2016, 12-19 July 2016.

Cohen, H., Sarie, I., Medlej, B., Bocquentin, F., Toledano, T., Hershkovitz, I., Slon, V., 2012. Trauma to the skull: a historical perspective from the southern Levant (4300BCE-1917CE). Int. J. Osteoarchaeol. 24, 722–736. https://doi.org/10.1002/oa.2258.

Courtenay, L.A., Yravedra, J., Mate-González, M.Á., Aramendi, J., González-Aguilera, D., 2019. 3D analysis of cut marks using a new geometric morphometric methodological approach. Archaeol. Anthropol. Sci. 11, 651–665. https://doi.org/10.1007/s12520-017-0554-x.

De Reu, J., Plets, G., De Smedt, P., Bats, M., Cherretté, B., De Maeyer, W., Deconynck, J., Herremans, D., Laloo, P., Van Meirvenne, M., De Clercq, W., 2013. Towards a three-dimensional cost-effective registration of the archaeological heritage. J. Archaeol. Sci. 40 (2), 1108–1121. https://doi.org/10.1016/j.jas.2012.08.040.

De Reu, J., De Smedt, P., Herremans, D., Van Meirvenne, M., Laloo, P., De Clercq, W., 2014. On introducing an image-based 3D reconstruction method in archaeological excavation practice. J. Archaeol. Sci. 41, 251–262. https://doi.org/10.1016/j.jas.2013.08.020.

Dellepiane, M., Dell'Unto, N., Callieri, M., Lindgren, S., Scopigno, R., 2013. Archaeological excavation monitoring using dense stereo matching techniques. J. Cult. Herit. 14, 201–210. https://doi.org/10.1016/j.culher.2012.01.011.

Ducke, B., Score, D., Reeves, J., 2011. Multiview 3D reconstruction of the archaeological site at Weymouth from image series. Comput. Graph. 35, 375–382. https://doi.org/10.1016/j.cag.2011.01.006.

England, Historic, 2017. Photogrammetric Applications for Cultural Heritage. Guidance for Good Practice [online]. Swindon: Historic England.

Errickson, D., Grueso, I., Griffith, S.J., Setchell, J.M., Thompson, T.J.U., Gowland, R.L., 2012. Towards a best practice for the use of active non-contact surface scanning to record human skeletal remains from archaeological contexts. Int. J. Osteoarchaeol. 27, 650–661. https://doi.org/10.1002/oa.2587.

Evgenikou, V., Georgopoulos, A., 2015. Investigating 3D reconstruction methods for small artefacts. In: González-Aguilera, D., Remondino, F., Boehm, J., Kersten, T., Fuse, T. (Eds.), International Archives of the Photogrammetry, Remote Sensing & Spatial Information Sciences XL-5/W4, 2015 3D Virtual Reconstruction and Visualisation of Complex Architectures, pp. 101–108. Avila 25-27 February 2015.

Falkingham, P.L., 2012. Acquisition of high resolution 3D models using free, open-source, photogrammetric software. Palaeontol. Electron. 15 (1), 1–15.

Field, A., 2009. Discovering statistics using SPSS, 3rd Edition. Sage Publications Ltd, London.

Fiorato, V., Boylston, A., Knüsel, C., 2000. Blood Red Roses, second ed. Oxbow Books, Oxford.

Fryer, J.G., Mitchell, H.L., Chandler, J.H., 2007. Applications of 3D measurement from images. Dunbeath: Whittles Publishing.

Gajski, D., Solter, A., Gašparović, M., 2016. Applications of macro photogrammetry in archaeology. In: Halounova, L., Šafář, V., Remondino, F., Hodač, J., Pavelka, K., Shortis, M., Rinaudo, F., Scaioni, M., Boehm, J., Rieke-Zapp, D. (Eds.), The International Archives of the Photogrammetry, Remote Sensing & Spatial Information Sciences, Volume XLI-B5. 2016 XXIII ISPRS congress, Prague, pp. 263–266. https://doi.org/10.5194/isprsarchives-XLI-B5-263-2016, 12-19 July 2016.

Gallo, A., Muzzupappa, M., Bruno, F., 2014. 3D reconstruction of small sized objects from a sequence of multi-focused images. J. Cult. Herit. 15, 173–182. https://doi.org/10.1016/j.culher.2013.04.009.

Giuffra, V., Pejrani Baricco, L., Subbrizio, M., Fornaciari, G., 2015. Weapon-related cranial lesions from medieval and renaissance Turin, Italy. Int. J. Osteoarchaeol. 25, 690–700. https://doi.org/10.1002/oa.2334.

Granshaw, S.I., 2016. Photogrammetric terminology: Third edition. The Photogrammetric Record 31 (154), 210–251.

Harten-Buga, H., Schwinning, M., Brinker, U., Lidke, G., Terberger, T., Jantzen, D., Nikulka, F., Orschiedt, J., 2018. Micro-traces of a major bronze age conflict: digital trauma analysis in the Tollense valley, Germany. PAST: The Newsletter of the Prehist. Soc. 90, 1–4.

James, M.R., Robson, S., Smith, M.W., 2017a. 3-D uncertainty-based topographic change detection with structure-from-motion photogrammetry: precision maps for ground control and directly georeferenced surveys. Earth Surf. Process. Landforms 42, 1769–1788. https://doi.org/10.1002/esp.4125.

James, M.R., Robson, S., d'Oleire-Oltmanns, S., Niethammer, U., 2017b. Optimising UAV topographic surveys processed with structure-from-motion: ground control quality, quantity and bundle adjustment. Geomorphology 280, 51–66. https://doi.org/10.1016/j.geomorph.2016.11.021.

Kasser, M., Egels, Y., 2002. Digital Photogrammetry. Taylor & Francis, London.

Konecny, G., 1985. The international society for photogrammetry and remote sensing – 75 years old, or 75 years young. Photogramm. Eng. Rem. Sens. 51 (7), 919–933.

Lauria, G., Sineo, L., Ficcara, S., 2022. A detailed method for creating digital 3D models of human crania: an example of close-range photogrammetry based on the use of Structure-from-Motion (SfM) in virtual anthropology. Archaeol. Anthropol. Sci. 14 (42) https://doi.org/10.1007/s12520-022-01502-9.

Lillesand, T., Kiefer, R.W., Chipman, J., 2015. Remote Sensing and Image Interpretation, seventh ed. John Wiley & Sons, Hoboken.

Linder, W., 2016. Digital Photogrammetry: A Practical Course, fourth ed. Springer, Berlin.

Loe, L., Boyle, A., Webb, H., Score, D., 2014. 'Given to the Ground': A Viking Age Mass Grave on Ridgeway Hill, Weymouth. Dorset Natural History and Archaeological Society Monograph Series No. 22. Dorset Natural History and Archaeological Society, Dorchester.

Luhmann, T., Robson, S., Kyle, S., Boehm, J., 2013. Close-range Photogrammetry and 3D Imaging. De Gruyters, Berlin.

Lussu, P., Marini, E., 2020. Ultra close-range digital photogrammetry in skeletal anthropology: A systematic review. PLoS ONE 15 (4), e0230948.

Magnani, M., Douglass, M., Schroder, W., Reeves, J., Braun, D.R., 2020. The digital revolution to come: photogrammetry in archaeological practice. Am. Antiq. 85 (4), 737–760. https://doi.org/10.1017/aaq.2020.59.

Mallison, H., Wings, O., 2014. Photogrammetry in paleontology – a practical guide. J. Paleontol. Tech. 12, 1–31.

Maté González, M.Á., Yravedra, J., González-Aguilara, D., Palomeque-González, J.F., Domínguez-Rodrigo, M., 2015. Micro-photogrammetry characterization of cut marks on bones. J. Archaeol. Sci. 62, 128–142. https://doi.org/10.1016/j.jas.2015.08.006.

Maté-González, M.Á., Aramendi, J., Yravedra, J., Blasco, R., Rosell, J., González-Aguilara, D., Domínguez-Rodrigo, M., 2017. Assessment of statistical agreement of three techniques for the study of cut marks: 3D digital microscopy, laser scanning confocal microscopy and micro-photogrammetry. J. Microsc. 267 (3), 356–370. https://doi.org/10.1111/jmi.12575.

Maté-González, M.Á., Palomeque-González, J.F., Yravedra, J., González-Aguilara, D., Domínguez-Rodrigo, M., 2018. Micro-photogrammetric and morphometric differentiation of cut marks on bone using metal knives, quartzite, and flint flakes. Archaeol. Anthropol. Sci. 10 (4), 805–816. https://doi.org/10.1007/s12520-016-0401-5.

McCarthy, J., 2014. Multi-image photogrammetry as a practical tool for cultural heritage survey and community engagement. J. Archaeol. Sci. 43, 175–185. https://doi.org/10.1016/j.jas.2014.01.010.

McQuaid, G., Millar, P., Woodward, D., Friel, S., 2013. Use of close range photogrammetry to assess the micro-texture of asphalt surfacing aggregate. In: International Journal of Pavements Conference. São Paolo, pp. 9–10. December 2013.

Morgan, B., Ford, A.L.J., Smith, M.J., 2019. Standard methods for creating digital skeletal models using structure-from-motion photogrammetry. Am. J. Phys. Anthropol. 169 (1), 152–160. https://doi.org/10.1002/ajpa.23803.

Nikon, 2020a. DSLR Cameras. https://www.nikon.co.uk/en_GB/products/category_pages/digital_cameras/category_slr.page. (Accessed 23 March 2020).

Nikon, 2020b. https://www.nikon.co.uk/en_GB/product/nikkor-lenses/auto-focus-lenses/fx/single-focal-length/af-s-micro-nikkor-60mm-f-2-8g-ed. (Accessed 23 March 2020). AF-S Micro NIKKOR 60mm f/2.8G ED.

Núñez, M.A., Buill, F., Edo, M., 2013. 3D model of the Can Sadurní cave. J. Archaeol. Sci. 40, 4420–4428. https://doi.org/10.1016/j.jas.2013.07.006.

Olson, B.R., Placchetti, R.A., Quartermaine, J., Killebrew, A.E., 2013. The tel akko total archaeology project (akko, Israel): assessing the suitability of multi-scale 3D field recording in archaeology. J. Field Archaeol. 38 (3), 244–262. https://doi.org/10.1179/0093469013Z.00000000056.

Oniga, V.-E., Breaban, A.-I., Statescu, F., 2018. Determining the optimum number of ground control points for obtaining high precision results based on UAS images. In: Gitas, I. (Ed.), The 2nd International Electronic Conference on Remote Sensing, pp. 352–362. https://doi.org/10.3390/ecrs-2-05165. Online. 22 March-5 April 2017.

Opitz, R.S., 2013. Appendix: Key technical terms. In: Opitz, R.S., Cowley, D.C. (Eds.), Interpreting archaeological topography: Airborne laser scanning, 3D data and ground observation. Oxbow Books, Oxford, pp. 266–268.

Papworth, H., Ford, A., Welham, K., Thackray, D., 2016. Assessing 3D metric data of digital surface models for extracting archaeological data from Archive stereo-aerial photographs. J. Archaeol. Sci. 72, 85–104. https://doi.org/10.1016/j.jas.2016.05.005.

Porter, S.T., Roussel, M., Soressi, M., 2016. A simple photogrammetry rig for the reliable creation of 3D artifact models in the field: lithic examples from the Early Upper Paleolithic sequence of Les Cottés (France). Adv. Archaeol. Pract. 4 (1), 71–86. https://doi.org/10.7183/2326-3768.4.1.71.

Remondino, F., 2011. Heritage recording and 3D modelling with photogrammetry and 3D scanning. Rem. Sens. 3, 1104–1138. https://doi.org/10.3390/rs3061104.

Rodríguez-Martín, M., Rodríguez-Gonzálvez, P., Lagüela, S., Gonzálvez-Alguilera, D., 2016. Macro-photogrammetry as a tool for the accurate measurement of three-dimensional misalignment in welding. Autom. ConStruct. 71, 189–197. https://doi.org/10.1016/j.autcon.2016.08.016.

Sanz-Ablanedo, E., Chandler, J.H., Rodríguez-Pérez, J.R., Ordóñez, C., 2018. Accuracy of unmanned aerial vehicle (UAV) and SfM photogrammetry survey as a function of the number and location of ground control points used. Rem. Sens. 10 (10), 1606. https://doi.org/10.3390/rs10101606.

Sapirstein, P., 2016. Accurate measurements with photogrammetry at large sites. J. Archaeol. Sci. 66, 137–145. https://doi.org/10.1016/j.jas.2016.01.002.

Sapirstein, P., 2018. A high-precision photogrammetric recording system for small artifacts. J. Cult. Herit. 31, 33–45. https://doi.org/10.1016/j.culher.2017.10.011.

Sapirstein, P., Murray, S., 2017. Establishing best practices for photogrammetric recording during archaeological fieldwork. J. Field Archaeol. 42 (4), 337–350. https://doi.org/10.1080/00934690.2017.1338513.

Smith, M.J., Brickley, M.B., 2004. Analysis and interpretation of flint toolmarks found in bones from west tump long barrow, gloucestershire. Int. J. Osteoarchaeol. 14, 18–33. https://doi.org/10.1002/oa.710.

Symes, S.A., L'Abbé, E.N., Chapman, E.N., Dirkmaat, D.C., 2012. Interpreting traumatic injury to bone in medicolegal investigations. In: Dirkmaat, D.C. (Ed.), A Companion to Forensic Anthropology. Wiley-Blackwell, Malden, pp. 340–389.

Tamminen, H.M., 2022. The Digital Dead: Virtual Modelling of Human Remains Using Photogrammetry for Presentation and Preservation by Record. PhD Thesis. Bournemouth University.

Tamminen, H.M., Ford, A., Welham, K., Smith, M.J., 2019. Vikings go digital: using the Ridgeway mass burial to investigate skeletal injuries in three dimensions. Proc. Dorset Nat. Hist. Archaeol. Soc. 140, 81–84.

Tamminen, H.M., Ford, A.L.J., Welham, K., Loe, L., Webb, H., Boyle, A., Smith, M.J., 2023. Residual energy dispersal fracturing: a newly proposed term for fractures propagating from sharp-force trauma. Am. J. Biol. Anthropol. 1–11.

Vazzana, A., Scalise, L.M., Traversari, M., Figus, C., Apicella, S.A., Buti, L., Oxilia, G., Sorrentino, R., Pellegrini, S., Matteucci, C., Calcagnile, L., Savigni, R., Feeney, R.N. M., Gruppioni, G., Benazzi, S., 2018. A multianalytic investigation of weapon-related

injuries in a late antiquity necropolis, Mutina, Italy. J. Archaeol. Sci.: Report 17, 550–559. https://doi.org/10.1016/j.jasrep.2017.12.009.
Verhoeven, G., 2011. Taking computer vision aloft – archaeological three-dimensional reconstructions from aerial photographs with PhotoScan. Archaeol. Prospect. 18, 67–73. https://doi.org/10.1002/arp.399.
Verhoeven, G., Taelman, D., Vermeulen, F., 2012. Computer vision-based orthophoto mapping of complex archaeological sites: the ancient quarry of Pitaranha (Portugal-Spain). Archaeometry 54 (6), 1114–1129. https://doi.org/10.1111/j.1475-4754.2012.00667.x.
Versi, E., 1992. "Gold standard" is an appropriate term. Br. Med. J. 305, 187.
Walsh, T., 2018. Fuzzy gold standards: approaches to handling an imperfect reference standard. J. Dent. 74, S47–S49. https://doi.org/10.1016/j.jdent.2018.04.022.
Westoby, M.J., Brasington, J., Glasser, N.F., Hambrey, M.J., Reynolds, J.M., 2012. 'Structure-from-motion' photogrammetry: a low-cost, effective tool for geoscience applications. Geomorphology 179, 300–314. https://doi.org/10.1016/j.geomorph.2012.08.021.
Wolf, P.R., Dewitt, B.A., Wilkinson, B.A., 2014. Elements of Photogrammetry with Applications in GIS [online], fourth ed. McGraw-Hill, New York.
Yravedra, J., García Vargas, E., Maté-González, M.Á., Palomeque-González, J.F., Vallés-Iriso, J., Matesanz-Vincente, J., González-Aguilara, D., Domínguez-Rodrigo, M., 2017. The use of micro-photogrammetry and geometric morphometrics for identifying carnivore agency in bone assemblages. J. Archaeol. Sci.: Rep. 14, 106–115.
Zawieska, D., Markiewocz, J., Łuba, M., 2019. Macro photogrammetry in inventory of historic engravings at the royal castle in Warsaw. In: Cardaci, A., Fassi, F., Remondino, F. (Eds.), The International Archives of the Photogrammetry, Remote Sensing & Spatial Information Sciences Volume XLII-2/W9, 8th International Workshop 3D-ARCH "3D Virtual Reconstruction and Visualization of Complex Architectures" https://doi.org/10.5194/isprs-archives-XLII-2-W9-795-2019. Bergamo 6-8 February 2019. 795-800.